Organic Aerosol Growth Mechanisms and Their Climate-Forcing Implications

Steven F. Maria,[1] Lynn M. Russell,[3]* Mary K. Gilles,[4] Satish C. B. Myneni[2,5]

Surface- and volume-limited chemical reactions on and in atmospheric aerosol particles cause growth while changing organic composition by 13 to 24% per day. Many of these particles contain carbonaceous components from mineral dust and combustion emissions in Africa, Asia, and North America and reveal reaction rates that are three times slower than those typically used in climate models. These slower rates for converting from volatile or hydrophobic to condensed and hygroscopic organic compounds increase carbonaceous particle burdens in climate models by 70%, producing organic aerosol climate forcings of as much as −0.8 watt per square meter cooling and +0.3 watt per square meter warming.

Aerosol particles enter Earth's atmosphere by direct emission of particles and by condensation of vapor-phase species. Heterogeneous and multiphase reactions in the atmosphere change chemical and physical properties of aerosol particles, but these processes are not understood well enough to predict accurately the evolution of the gas and particle-phase

[1]Department of Chemical Engineering, [2]Department of Geosciences, Princeton University, Princeton, NJ 08544, USA. [3]Scripps Institution of Oceanography, University of California San Diego, La Jolla, CA 92093, USA. [4]Chemical Sciences Division, [5]Advanced Light Source, Lawrence Berkeley National Laboratory, Berkeley, CA 94720, USA.

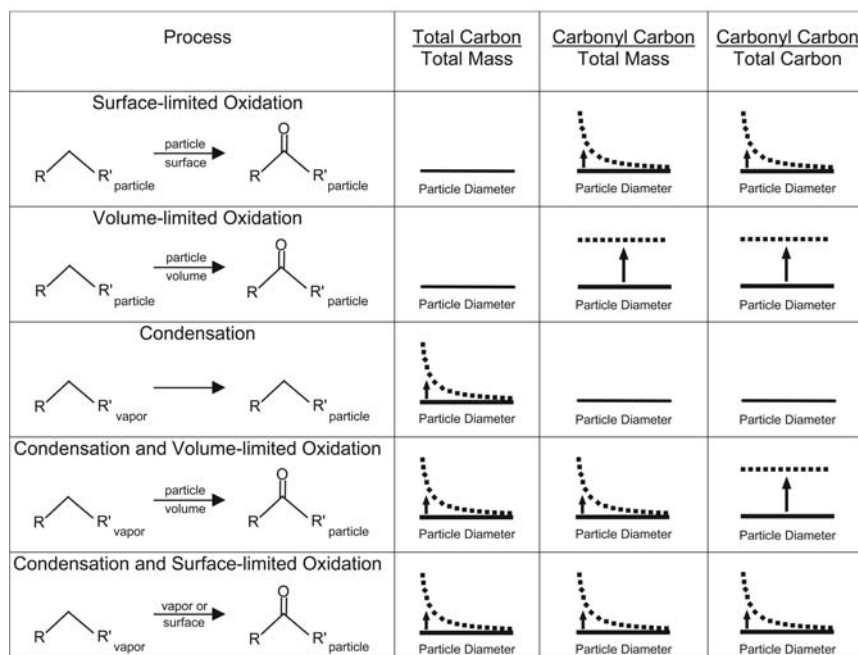*To whom correspondence should be addressed. E-mail: lmrussell@ucsd.edu

composition of the troposphere (1). Carbonaceous aerosol particles compose ~37% of global submicrometer particle emissions (2), yet climate models have used an oxidation reaction rate equivalent to 60% of organic particle mass per day for these particles because atmospheric observations have not been available (3, 4). This assumption controls the associated lifetime, burden, and climate forcing predicted for atmospheric carbonaceous particles.

Because gas-to-particle conversion and heterogeneous chemistry control the composition of carbonaceous particles in ways that are poorly understood, the organic composition of atmospheric particles is also not well known (5). The oxidation of vapor-phase organic com-

pounds, in which the number of alkyl bonds is reduced and the number of alcohol and carbonyl bonds is increased, produces compounds that may have sufficiently low vapor pressures to condense onto preexisting particle surfaces to form secondary organic aerosol (SOA). This condensation pathway accounts for an estimated 10% of global organic aerosol (4) and increases the fractional concentrations of the condensing species more rapidly for smaller than for larger particles because of larger surface area–to–volume ratios in smaller particles.

Condensed organic compounds originating from the vapor phase or from direct particulate emissions can become oxidized through heterogeneous reactions that are surface-limited or volume-limited (6). Typically these mechanisms are represented by a single lumped rate in climate models (4). Mixtures of large molecular-weight organic compounds with elemental carbon are also oxidized by atmospheric reactions. Volume-limited oxidation occurs when particle-phase diffusion of reactants is fast compared with the kinetics of chemical reaction. A uniform reaction extent results in an equally increased carbonyl carbon concentration for all particles regardless of size. Surface-limited oxidation may indicate efficient surface reactivity or highly viscous or solid aerosols, and the localization of the reaction at the surface results in larger concentrations of carbonyl carbon for smaller aerosol particles with larger surface area–to–volume ratios than for larger particles. Condensation of organic compounds from the gas phase to the particle phase, oxidation of those organic compounds on particles surfaces, and oxidation of compounds that have diffused into particle volumes, as well as combina-

Fig. 1. Theoretical diagrams showing the effects of five oxidation and condensation mechanisms on organic mass composition ratios as functions of particle diameter. In each diagram, the vertical axis represents a unitless ratio and the horizontal axis represents particle size with diameters increasing toward the right for the size range from 0.4 to 5 μm in diameter. The exact size scale for each diagram varies with atmospheric parameters including processing time, temperature, and vapor-phase concentrations of the reacting or condensing species. Condensation, volume-limited oxidation, and surface-limited oxidation mechanisms can be distinguished with use of the three STXM variables shown here: the total carbon–to–total mass ratio, the carbonyl carbon–to–total mass ratio, and the carbonyl carbon–to–total carbon ratio. In all diagrams, R and R′ indicate aliphatic chains, hydrogen atoms, or alcohol groups. Subscripts refer to the reactant phase, and arrow labels indicate the reaction phase where oxidation occurs. Condensation followed by surface-limited vapor-phase reaction has the same organic composition dependence on size as the condensation of oxygenated organic compounds oxidized in the vapor phase. The particle-phase reaction of vapor-phase reactants can occur if vapor-phase reactants absorb or condense onto aerosol particles before reacting.
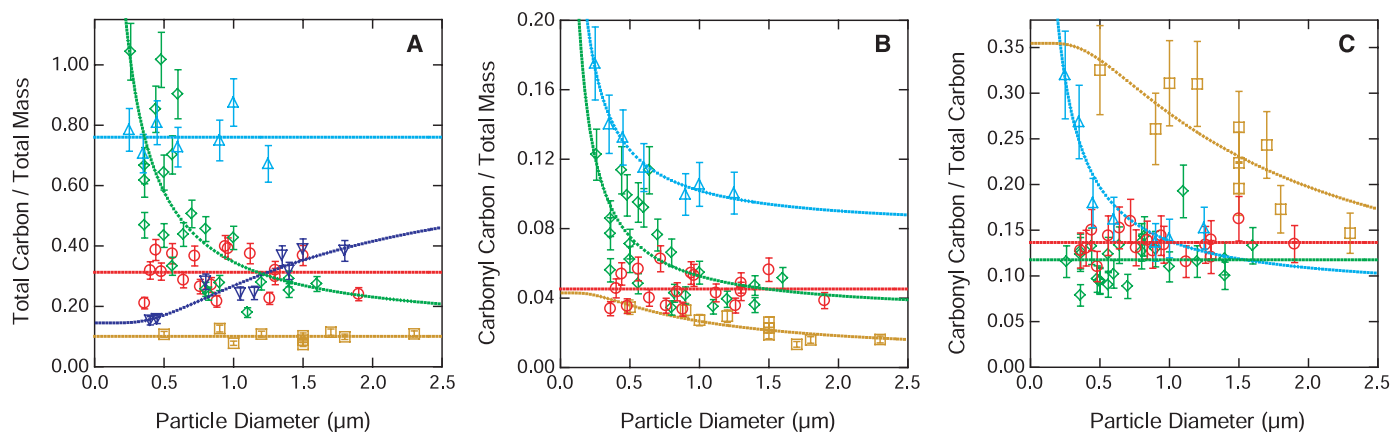
Fig. 2. For individual particles, the (**A**) total carbon–to–total mass ratio, (**B**) carbonyl carbon–to–total mass ratio, and (**C**) carbonyl carbon–to–total carbon ratio are shown as a function of particle diameter. Light blue triangles represent the organic mode of Asian mixed combustion aerosol particles collected during the Aerosol Characterization Experiment (ACE)–Asia project over the Sea of Japan on 27 April 2001, dark blue inverted triangles [only in (A)] represent the sulfate mode of Asian mixed combustion aerosol particles collected over the Sea of Japan on 27 April 2001, brown squares represent African mineral dust collected over the Caribbean Sea on 21 July 2000, red circles represent eastern U.S. combustion particles collected in New Jersey under clear conditions on 12 August 2003, and green diamonds represent eastern U.S. combustion particles collected in New Jersey under foggy conditions on 7 August 2003. Error bars represent the uncertainty associated with the calibration from absorbance ratios to mass ratios. Dotted lines represent curve fits to the data. The sulfate mode of the Asian mixed combustion particles has been removed from (B) and (C) because the large variability associated with this mode masks any underlying atmospheric processes. These particles did not show a dependence of organic composition with size that was consistent with any single dominant condensation or oxidation mechanism.

tions of these processes, are summarized (Fig. 1). The reaction mechanisms and the phase origin of the reactants can be distinguished by using size-resolved aerosol chemical composition measurements of organic functional groups.

Soft x-ray spectromicroscopy studies in the transmission mode (scanning transmission x-ray microscopy, or STXM) can detect organic functional groups within individual particles with a resolution below 0.1 µm (7). By using this technique, data from four atmospheric aerosol samples (Asian mixed combustion over the Sea of Japan, African mineral dust over the Caribbean Sea, and U.S. combustion in New Jersey) were analyzed (Fig. 2). Details for each sample are also summarized (Fig. 3). For each aerosol sample, two-dimensional maps of particle composition and morphology were compiled from STXM measurements (8). In Fig. 2, STXM absorbance ratios were converted to absolute mass ratios by using the Fourier transform infrared–measured compositions of simultaneously collected bulk submicrometer aerosol samples for calibration (9). Spatial distributions of measured composition ratios (Fig. 4) illustrate four different particle morphologies and mixing states. The four samples provide examples of the aerosol organic reaction mechanisms described in Fig. 1.

Evidence of surface-limited oxidation is reflected in the chemical composition of Asian mixed combustion aerosol collected at 1500 m over the Sea of Japan. This sample contains two aerosol modes evident from the particle maps in Fig. 4, A and B, and the total carbon–to–total mass ratio in Fig. 2A: a carbonaceous mode and a mode containing

Fig. 3. Source type, STXM composition, and mechanism information for the four aerosol samples. All compositions are mass-average values from single-particle measurements. The Asian mixed combustion aerosol included two distinct modes, and the STXM results shown here are for the organic mode only. The oxidation rate in mass percent per day was calculated by using back trajectories to estimate aerosol age and assuming a primary carbonyl–to–total carbon ratio of 10%. This value was chosen by extrapolating time since emission and composition data for the four aerosol samples to the time of emission.
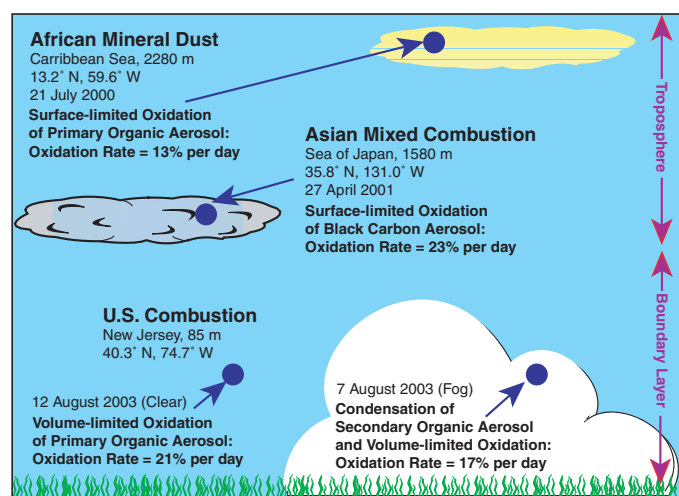

very low carbon concentrations. The carbonaceous mode composition has a size dependence in Fig. 2, B and C, and does not in Fig. 2A, consistent with a surface-limited oxidation mechanism (Fig. 1). The lack of size dependence of the total carbon–to–total mass ratio suggests that organic compounds were incorporated in the particle phase before the particles were emitted from their sources.

In the Asian mixed combustion particles, the strong absorption by carbon-carbon double bonds is consistent with products of incomplete combustion including polycyclic aromatic hydrocarbons and graphitic elemental carbon, components whose light-absorbing properties have earned the popular appellation of black carbon (abbreviated in

this work as BC). The particles were sampled in dry conditions more than 30 hours after emission (8) and may have been crystalline or amorphous solids. Particle composition is consistent with an oxidation rate of 24% of carbon mass per day, increasing the carbonyl–to–total carbon ratio by 5.5% per day. In Fig. 4H, the organic mode particles have larger carbonyl carbon–to–total carbon ratios at particle edges, with ratios near 0.2 occurring exclusively in edge regions. Bulk filter analysis shows that the Asian mixed combustion submicrometer particles consist of organic compounds and sulfate with substantial BC and almost no dust (10). The mode with low carbon concentrations is probably largely sulfate. Particles from both modes are

Fig. 4. Two-dimensional spectrally resolved maps of organic composition for particles representative of the four aerosol samples shown in Fig. 2. The total carbon–to–total mass ratios are plotted [(**A**),(**C**),(**E**), and (**G**)], demonstrating ratios of 0.02 to 0.2 (dark blue), 0.2 to 0.4 (yellow), 0.4 to 0.6 (orange), 0.6 to 0.8 (green), and >0.8 (light blue). The carbonyl–to–total carbon ratio is plotted [(**B**), (**D**), (**F**), and (**H**)], demonstrating ratios of 0.02 to 0.08 (dark blue), 0.08 to 0.16 (yellow), 0.16 to 0.24 (orange), 0.24 to 0.32 (green), and >0.32 (light blue). For chemically heterogeneous particles, regions of enhanced carbon and carbonyl concentrations can be identified as orange, green, or light blue areas in the plots shown here. The samples shown are [(A) and (B)] Asian combustion over the Sea of Japan on 27 April 2001, [(C) and (D)] African mineral dust over the Caribbean Sea on 21 July 2000, [(E) and (F)] eastern U.S. combustion in New Jersey on 12 August 2003, and [(G) and (H)] eastern U.S. combustion during fog in New Jersey on 7 August 2003. For all panels, black outlines indicate regions where the total mass is above the detection limit. The total mass detection limit and the particle edges are effectively coincident to within the precision of the STXM measurement. White regions indicate that total carbon or carbonyl carbon signatures are below detection.
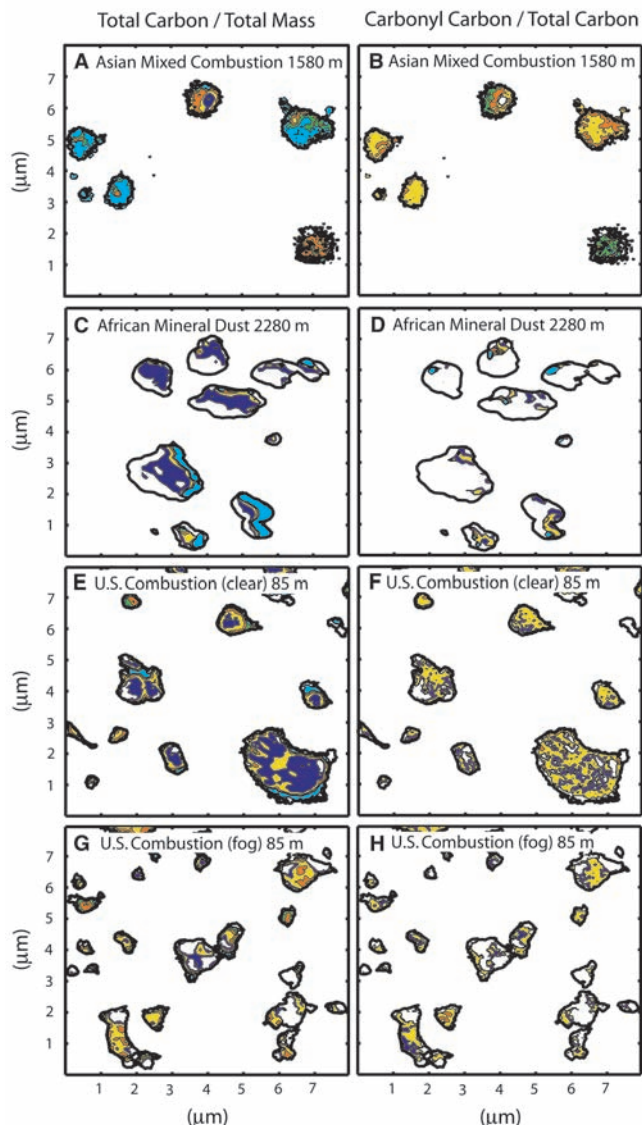
evident in Fig. 4A, with the low carbon mode containing 20 to 40% carbon by mass. The total carbon–to–total mass ratio of the low carbon mode increases with size (Fig. 2A).

Surface-limited oxidation signatures are also evident in the African mineral dust sample collected in the lower troposphere over the Caribbean Sea (*11*). The size dependence of the dust composition is similar to that of the carbonaceous mode of the Asian mixed combustion aerosol, providing evidence of surface-limited oxidation reactions without condensation processes (compare Fig. 2 to Fig. 1). The carbonyl carbon–to–total carbon ratio and the carbonyl carbon–to–total mass ratio both increase with decreasing particle size (Fig. 2, B and C), and the total carbon–to–total mass ratio is independent of particle size (Fig. 2A). The carbonyl carbon–to–total mass ratio is near 0.04 for 0.5-µm-diameter

particles and 0.02 for 2.0-µm-diameter particles, whereas the carbonyl carbon–to–total carbon ratio is near 0.3 for 0.5-µm-diameter particles and 0.2 for 2.0-µm-diameter particles. Surface-limited heterogeneous reactions have been reported previously in laboratory measurements on dust, including the uptake of acetaldehyde on mineral oxides (*12*), consistent with the observations for these particles.

The constant value of the total carbon–to–total mass ratio across all particle sizes (Fig. 2C) suggests that the organic compounds in the African mineral dust did not form by condensation. The organic carbon compounds, composing 10% of total mass (Fig. 2A), were most likely associated with the dust source and subsequently oxidized on the dust particles during transport. Spatial distributions (Fig. 4, C and D) demonstrate the resulting enhancement of carbonyl carbon concentra-

tions at the edges of particles. Carbonyl carbon is only above the detectable absorbance near particle edges, where it represents up to 40% of total carbon. From Fig. 2C, the carbonyl carbon–to–total carbon ratio of 0.3 for 0.5-µm-diameter particles is roughly three times larger than the average ratio of 0.1 for eastern U.S. combustion particles collected in the lower tropospheric boundary layer. The substantial oxidized fraction of carbon is consistent with the long atmospheric processing time associated with the dust particles that crossed the Atlantic before being sampled. The age of the mineral dust particles, sampled 5 days of transport from their source, is consistent with an oxidation reaction rate of 13% of organic compound mass per day, increasing the carbonyl carbon–to–total carbon ratio by 3% per day.

Volume-limited oxidation signatures are observable in the boundary layer U.S. combustion sample collected in New Jersey on 12 August 2003 in the absence of precipitation or fog. The chemical composition of this aerosol is constant across all measured sizes (Fig. 2) with an average carbonyl carbon–to–total carbon ratio of 0.1. The lack of sensitivity to particle size indicates that the carbon distribution was not controlled by surface-limited processes (compare Fig. 2 to Fig. 1). Relative humidity (RH) was high (>75%) on 12 August 2003 with particles containing some condensed water, and this aqueous phase may have facilitated the diffusion of reactants within particles for volume-limited reactions. The carbonyl–to–total carbon ratio is spatially uniform with similar values within particles and at particle edges (Fig. 4F), consistent with volume-limited oxidation. Isentropic back trajectories suggest that the boundary layer particles were collected at least 10 to 15 hours after emission (*8*). The estimated times since emission of these particles are consistent with an oxidation rate of 21% of organic compound mass per day, increasing the carbonyl carbon–to–total carbon ratio by 4.8% per day.

Volume-limited oxidation also occurred in the U.S. aerosol collected during a fog event on 7 August 2003 with similar emission sources as on 12 August 2003 (*8*). The size dependence of the total carbon–to–total mass ratio in Fig. 2A, near 0.5 for 0.8-µm-diameter particles and 1 for 0.3-µm-diameter particles, indicates organic condensation. The similar size dependence of the carbonyl carbon–to–total mass ratio in Fig. 2B, ranging up to 0.1 for a diameter of 0.3 µm, suggests that the condensed organic compounds were oxidized. The uniformity of the carbonyl carbon–to–total carbon ratio in Fig. 2C, 0.1 for all particle sizes, demonstrates that the organic compounds were oxidized uniformly regardless of the original phase or proximity to the particle surface. The spatial distribution of the carbonyl carbon–to–total carbon ratio (Fig. 4H) during the fog event shows fairly uniform values near 0.1, consist-

ent with Fig. 2C. These three trends of composition with size are consistent with condensation and volume-limited oxidation (Fig. 1).

On 7 and 12 August 2003, similar U.S. combustion sources produced particles with very different organic compositions: one with a strong size dependence and the other with none. The similarity of sources means that the observed differences in composition result from condensation and reaction processes that occurred after emission. The high RH and the presence of fog on 7 August 2003 suggest that most of the aerosol particles on that day contained substantial water. Condensation and volume-limited oxidation during fog events are consistent with the mechanism proposed for oxalic acid formation in cloud droplets (13). The close correspondence between the observed particle-composition size
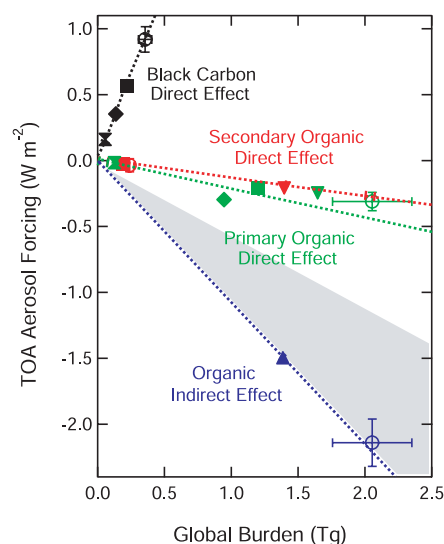

Fig. 5. Estimated TOA radiative forcing for four major effects of measured reaction rates for globally averaged carbonaceous aerosol burdens. Open circles show burden and forcing predictions calculated with use of the measured secondary organic aerosol (red), primary organic aerosol (green), and black carbon (black) oxidation rates. The carbonyl carbon–to–total carbon ratio of 0.3 was used for oxidation products, consistent with the measured ratio in particles dominated by oxidation products (aged African mineral dust particles and small condensation-dominated eastern U.S. combustion particles from 7 August 2003 in Fig. 2). Error bars represent the range of predictions associated with carbonyl–to–total carbon ratios from 0.2 to 0.5. Dotted lines are linear fits to the model predictions for each type of forcing. Solid symbols represent burden and forcing predictions, with squares (4), diamonds (17), inverted triangles (18), hourglasses (19), and triangles (16) representing carbonaceous aerosol burdens and TOA forcing from published estimates. TOA forcing estimates were extrapolated linearly from modeled values (4). The gray region indicates the large uncertainty associated with the indirect effect of organic aerosol, bounded by the estimate given here.

dependence during the fog event and the expected theoretical relationships for condensation (Fig. 2, A and B) and volume-limited oxidation (Fig. 2C) provides evidence supporting this pathway for forming the organic fraction of this aerosol. The particle ages are consistent with an SOA formation rate equivalent to 17% of the primary organic compound mass per day, increasing the carbonyl carbon–to–total carbon ratio by 4% per day.

The four aerosol chemical signatures illustrate differences in atmospheric processing, with evidence for four mechanisms of condensation and reaction in the atmosphere. Volume-limited oxidation reactions were observed in boundary layer aerosol in which particles were largely aqueous. Surface-limited oxidation reactions were observed in particles at higher altitudes where lower RH and insoluble components were present. All four distinct aerosol compositions from different regions and with competing reaction mechanisms consistently demonstrate an oxidation rate that is a factor of 3 or more lower than the values currently used in climate model calculations. Because oxidation is the removal mechanism for hydrophobic organic and BC particles in climate models (4), larger predicted carbonaceous aerosol lifetimes and burdens result from the slower oxidation rates.

The direct effects of carbonaceous aerosol cause cooling by light scattering and warming by absorption, both of which increase nearly proportionally with the aerosol burden (4). The carbonyl groups associated with organic molecules exert influence on cloud properties (14), affecting cloud formation in what is termed an indirect forcing. Figure 5 shows simple estimates of changes in global burdens and associated top-of-atmosphere (TOA) forcings for the measured oxidation rates of 24% per day for BC and 13 to 21% for organic aerosol. The estimated direct effects assume constant hygroscopicity and scavenging with organic composition. More detailed calculations including the changes in these properties are not possible because an accurate global characterization of the variability of these properties with location and oxidation state does not exist.

The much slower oxidation rates mean that organic aerosol will be less hygroscopic, reflecting more radiation because of increased atmospheric lifetimes and an estimated 70% increase of the organic aerosol burden. This change in average SOA, primary organic aerosol, and BC burdens is calculated from the atmospheric oxidation rates of the samples measured here with use of a global model of parameterized burden derived from detailed climate model calculations (4). By incorporating similar parameterizations of the direct and indirect effects, the result is a direct organic aerosol forcing increase of up to –0.1 W m^{-2}, an indirect forc-

ing increase of up to –0.7 W m^{-2} (15), and a BC forcing increase of up to +0.3 W m^{-2} (Fig. 5). The combined increases of cooling by 47% and warming by 61% represent an absolute difference of 1.1 W m^{-2} associated with uncertainties in the oxidation rate of carbonaceous aerosols, comparable to the total uncertainty in aerosol forcing and half of the magnitude of the forcing change from doubling CO$_2$ (+2.2 W m^{-2}).

References and Notes

1. A. R. Ravishankara, *Science* **276**, 1058 (1997).
2. V. Ramaswamy *et al.*, *Climate Change 2001: The Scientific Basis. Contribution of Working Group I to the Third Assessment Report of the Intergovernmental Panel on Climate Change* (Cambridge Univ. Press, New York, 2001), pp. 289–416.
3. W. F. Cooke, C. Liousse, H. Cachier, J. Feichter, *J. Geophys. Res.* **104**, 22137 (1999).
4. S. H. Chung, J. H. Seinfeld, *J. Geophys. Res.* **107**, 10.1029/2001JD000397 (2002).
5. E. E. Gard *et al.*, *Science* **279**, 1184 (1998).
6. D. R. Worsnop, J. W. Morris, Q. Shi, P. Davidovits, C. E. Kolb, *Geophys. Res. Lett.* **29**, 10.1029/2002GL015542 (2002).
7. L. M. Russell, S. F. Maria, S. C. B. Myneni, *Geophys. Res. Lett.* **29**, 10.1029/2002GL014874 (2002).
8. Materials and methods are available as supporting material on *Science* Online.
9. The average total carbon–to–total mass absorption ratio for each STXM sample was calibrated to the bulk aerosol organic carbon mass fraction. This calibration is rigorous for 0.2- to 2.0-μm-diameter STXM particle populations with mass average compositions that are equivalent to the submicrometer aerosol mass average measured for each sample.
10. S. F. Maria *et al.*, *J. Geophys. Res.* **108**, 10.1029/2003JD003703 (2003).
11. T. J. Garrett, L. M. Russell, V. Ramaswamy, S. F. Maria, B. J. Huebert, *J. Geophys. Res.* **108**, 10.1029/2002JD002228 (2003).
12. V. H. Grassian, *Int. Rev. Phys. Chem.* **20**, 467 (2001).
13. K. K. Crahan, D. Hegg, D. S. Covert, H. Jonsson, *Atmos. Environ.* **38**, 3757 (2004).
14. R. J. Charlson *et al.*, *Science* **292**, 2025 (2001).
15. Organic compounds may account for up to 63% of cloud condensation nuclei (16), corresponding to an indirect forcing estimated to be –1.5 W m^{-2}. The longer lifetime of hydrophobic organic compounds predicted here would magnify this effect, increasing the organic fraction of cloud droplets from 63% to 75% and increasing the global organic indirect effect to –2.2 W m^{-2} (2). This estimated indirect effect gives an order-of-magnitude calculation by extending a limited set of observations and provides an upper bound on the forcing magnitude (gray region in Fig. 5).
16. T. Novakov, J. E. Penner, *Nature* **365**, 823 (1993).
17. D. Koch, *J. Geophys. Res.* **106**, 20311 (2001).
18. M. Kanakidou, K. Tsigaridis, F. J. Dentener, P. J. Crutzen, *J. Geophys. Res.* **105**, 9243 (2000).
19. W. F. Cooke, V. Ramaswamy, P. Kasibhatla, *J. Geophys. Res.* **107**, 10.1029/2001JD001274 (2002).
20. Support for this research was provided by NSF grant ATM-0408501 and the James S. McDonnell Foundation. The authors thank A. L. D. Kilcoyne and Lawrence Berkeley National Laboratory for usage and support of Advanced Light Source Beamline 5.3.2.